2005-0689

43rd Aerospace Sciences Meeting, 10-13 January 2005, Reno, Nevada

Laminar Heating Validation of the OVERFLOW Code

Randolph P. Lillard *

Purdue University, West Lafayette, IN 47907-1282, US

Kevin M. Dries †

NASA Johnson Space Center, Houston, TX, 77058, US

OVERFLOW, a structured finite difference code, was applied to the solution of hypersonic laminar flow over several configurations assuming perfect gas chemistry. By testing OVERFLOW's capabilities over several configurations encompassing a variety of flow physics a validated laminar heating was produced. Configurations tested were a flat plate at 0 degrees incidence, a sphere, a compression ramp, and the X-38 re-entry vehicle. This variety of test cases shows the ability of the code to predict boundary layer flow, stagnation heating, laminar separation with re-attachment heating, and complex flow over a three-dimensional body. In addition, grid resolutions studies were done to give recommendations for the correct number of off-body points to be applied to generic problems and for wall-spacing values to capture heat transfer and skin friction. Numerical results show good comparison to the test data for all the configurations.

Nomenclature

a	sound speed, m/s
C_f	skin friction coefficient
C_h	heat transfer coefficient
C_p	pressure coefficient
M	Mach number
P	static pressure, Pa
q	heat flux per unit area, W/m^2
r	recovery factor, 0.845 laminar, 0.89 turbulent
Re/m	Reynolds number per unit meter, $1/m$
S_t	Stanton number, $q_w/\rho_\infty U_\infty C_p(rT_{aw} - T_w)$
T	static temperature, K
U	freestream velocity, m/s
x, y, z	cartesian body axes, m
μ	dynamic viscosity, $kg/m \cdot s$
ρ	density, kg/m^3
τ_{ij}	stress tensor, Pa
Δz	wall spacing, m
ξ	nondimensionl streamwise coordinate direction

*Research Assistant, Student Member, AIAA

†Aerospace Engineer, NASA/JSC, 2101 NASA Parkway, Houston, TX

η nondimensional off-body coordinate direction

Subscript

aw adiabatic wall

t total conditions

w wall conditions

∞ freestream conditions

I. Introduction

This work was carried out to begin development of a capability to model high-speed compressible flows with laminar flow regions over complex re-entry vehicles. Stagnation heating and laminar boundary layer flow represent two of the most important phenomenons in the design of re-entry vehicles. Heat flux to the surface is an important factor in the selection and sizing of the vehicle's Thermal Protection System (TPS). This study was designed to evaluate the capability of the OVERFLOW code[1,2] to predict laminar heating in stagnation regions and laminar boundary layers with attached and separated flow. Results (heat transfer, skin friction, and pressure) were compared to wind tunnel measurements of a flat plate, sphere, 2D compression ramp, and the X-38 re-entry vehicle. The simple test cases (sphere, flat plate, and 2D compression ramp) provide a step by step approach to build up to a full 3D flight vehicle.

The OVERFLOW code utilizes finite differencing (central spaced) with matrix dissipation and multigrid capability along with the ability to compute on overset grids.[3] Overset grid capability makes OVERFLOW ideal for predicting flowfields over very complex geometries. Olsen et al[4] verified the applicability of the OVERLFOW code to hypersonic flowfields by looking at several inviscid and viscous flowfields. A limited set of perfect gas laminar heating predictions were done. Olsen presented constants for the Swanson/Turkel matrix dissipation model[5] that mimic a Total Variation Dimenishing (TVD) upwind biased scheme. For pure central differencing on a per grid point basis, the speedup over an upwinded TVD scheme is a factor of 2. The matrix dissipation in OVERFLOW takes advantage of the speed of central differencing while in regions of flow discontinuities mimics the behavior of an upwinded TVD scheme. The scope of this work was to continue the validation of OVERFLOW's laminar heating capability by looking at a larger range of test cases and examining any depenencies with grid resolution and wall spacing.

A. Background

OVERFLOW is a structured (overset) grid, Navier-Stokes flow solver. It uses a finite-difference formulation, with flow quantities stored at the grid nodes. OVERFLOW has central- and Roe upwind-difference options, and uses a diagonalized, implicit approximate factorization scheme for the time advance. Local timestepping, multigrid techniques and grid sequencing are all used to accelerate convergence to a steady state. Thin-layer viscous terms are computed in wall-normal direction by default. In this study, 2nd-order central differencing with Swanson/Turkel type 2nd/4th-order matrix dissipation was utilized. With correct parameters, this scheme eliminates the 'carbuncle' problem of blunt body flowfields. For a complete discussion of the scheme see Olsen et al.[4]

B. Computational Method

Matrix dissipation allows for 4 parameters to be adjusted. As described in Swanson et al,[5] the 2nd and 4th order dissipation terms are κ_2 and κ_4. The second order term adds dissipation near shocks while the 4th order term adds dissipation in the boundary layer and other low pressure gradient regions. In OVERFLOW, the second and fourth order dissipation terms are DIS2 and DIS4, respectively. The two remaining terms are eigenvalue limiters, $V_{\epsilon_{eta}}$ and V_{ϵ_l}. Setting the eigenvalue limiters to unity will make the matrix dissipation scheme mimic a scalar dissipation scheme. In OVERFLOW, the eigenvalue limiters are VEPSN and VEPSL,

respectively. Provided the four parameters are chosen as listed below, the flowfield will converge high speed flows with strong shocks.

$$DIS2 = 2$$
$$DIS4 = .1$$
$$V_{\epsilon_\eta} = 0.3$$
$$V_{\epsilon_l} = 0.3$$

To begin the solution process, the flow was initialized to freestream values on a sequence of progressively finer grids until the finest grid level is obtained. Coarse grids are created internally to OVERFLOW by specifying a number of grid levels (three grid levels would be the original fine grid and a medium grid with every other grid point chosen and a coarse grid with every fourth grid point chosen). For this study, three or four grid levels were used depending on the case. Between 500 and 1000 coarse and medium iterations on each grid level were used to obtain a startup solution. During this initial startup process, the four parameters were changed to the following values:

$$DIS2 = 10$$
$$DIS4 = .2$$
$$V_{\epsilon_\eta} = 1.0$$
$$V_{\epsilon_l} = 1.0$$

By combining larger dissipation values along with scalar dissipation behavior and coarse grids the initial solution is obtained very quickly and efficiently. Although the shock is smeared, this startup process provides the correct shock location. Once the coarse and medium iterations are done, the four parameters are changed back to their correct values for the remainder of the run. For very complex geometries, it is sometimes necessary to ramp DIS2, DIS4, VEPSN, and VEPSL from their startup values to the correct values (an example being lowering DIS2 from 10 to 4 then to 2 by in sets of 500 iterations). Without ramping the parameters the solution may not converge in complex flow regions. For each computation, the solution was run until the heat transfer converged over the area of interest, convergence being less than 0.?????% change in heat transfer per iteration. This took between 9000 and 15000 iterations with the maximum CFL number generally set at 0.5. Local time stepping was used for all cases. Roe averaging was used to obtain the matrices in the dissipation model and multigrid sequencing was always utilized. Fine grid residual reduction of 5 to 8 orders of magnitude was typically seen.

II. Test Descriptions

The four test cases were chosen because of their variation of flow structure as well as Mach number. Freestream conditions for all the configurations are given in Table 1.

A. Flat Plate

The flat plate data was obtained in the Langley 20-inch Mach 6 wind tunnel[6] as part of a larger study to investigate the effects of $\frac{T_w}{T_o}$ variations on the onset of transition.[7] Langley's Mach 6 tunnel is a conventional blowdown facility with a 0.508 x 0.5207m rectangular test section. Electric heaters can vary the stagnation temperature up to 590K, and the normal operating stagnation pressure is approximately 7×10^5 to 3.7×10^6 Pa. The model was run at two angles of attack (0 and 8) to vary the boundary layer edge Mach number.

The flat plate model was 0.5334 meters long with a leading edge thickness of 3.81×10^{-5} meters. Liquid nitrogen was injected into coolant passages on the flat plate to reduce the surface temperature. The model was 0.3556 meters wide with 38 thermocouples and 7 pressure orifices (only 6 were functional in the test). Pressure transducers were calibrated to an accuracy of 0.25% of the full-scale reading. Uncertainty in the

Table 1. FREESTREAM CONDITIONS

Variable	Flat Plate	Sphere	2D Ramp	X38
Mach	6.0	10.19	11.68	5.94
Re_m	1.407×10^7	7.408×10^6	5.58×10^5	6.56×10^6
T_t (K)	503.333	2372.11	1827.17	505.37
T_∞ (K)	65	127.15	64.6	62.73
T_w (K)	100.6667	295.83	297.2	300
α	0	0	0	40
$\rho_\infty(\frac{kg}{m^3})$	0.11853	0.0283	0.00128	0.0291
P_∞ (Pa)	2211.56	1036.77	23.73	523.97

heat transfer data was inferred by comparing 3 runs at the same freestream condition. Data repeatability showed an uncertainty between 5% and 10%.

B. Sphere

Sphere data was obtained in Calspan's 96 inch Hypersonic Shock tunnel.[8] Test models were hemispherical and made of either brass, stainless steel, or aluminum depending on the test condition. The models were instrumented with platinum thin-film heat transfer consisting of a painted platinum thin-film on a pyrex insert. Thin film gauges have an accuracy of approximately 3% with a response time on the order of microseconds.

C. Compression Ramp

The compression ramp data[9] was obtained in Calspan's 96 inch Hypersonic Shock tunnel just as the sphere data. The model consisted of a 0.442 meter length flat plate followed by a 0.2692 meter wedge at 15 degrees incidence. There were 30 heat transfer gauges, 15 skin friction gauges, and 30 pressure gauges on the model. This compression ramp was used as a test case for reentry problems[10] thus a complete discussion with several different numerical results are available for comparison.

D. X38

X38 data was obtained in the same 20-Inch Mach 6 wind tunnel[6] as the flat plate data (although over 30 years later). Data was obtained by using phosphor thermography techniques.[11] This method uses ceramic models that are coated with phosphors that when illuminated with ultraviolet light, fluoresce in two regions of the visible spectrum. The fluorescence intensity is dependent on the surface temperature. By taking fluorescence intensity images with a color video camera and calibrating the temperature prior to the test, heat transfer can be calculated based on the surface temperature time histories.

The X38 model was 6" in length, 1.75% of the full-scale model. The published data is in the form of constant axial and longitudinal cuts.[11]

III. Grid Generation

Generating grids for compressible hypersonic applications can be a difficult task. The grids need to be created with sufficient grid density in the off-body direction to capture the boundary layer profile. In

Table 2. STRETCHING RATIO BY GRID TYPE

grid level	parabolic grid	finite radius
fine (169 pnts)	1.15	1.08
medium (85 pnts)	1.22	1.224
coarse (43 pnts)	1.56	1.4

addition, the inflow boundary must be aligned with the bow shock with several grid points to capture the shock correctly. For laminar heating, the Re_{cell}, defined in equation 1, defines the wall spacing quality.

$$Re_{cell} = \frac{\rho_w a_w \Delta z}{\mu_w} \tag{1}$$

Typically, Re_{cell} values between 1 and 5 are sufficient to capture the laminar wall properties.[12] Creating grids with constant Re_{cell} values requires several iterations to capture the correct wall properties. This is done by specifying an initial constant spacing over the vehicle, then the wall spacing is modified at each grid point as the run progresses until the desired Re_{cell} value is obtained. As the solution is iterated, the wall properties become more accurate and begin to converge and accurate Re_{cell} values are obtained. Appropriate value for OVERFLOW will be discussed. The grid generation was done with a hyperbolic grid generator to keep the grid lines orthogonal to the surface.

A. Flat Plate

For the flat plate study, two different grid topologies were generated, both with the (x,y,z) Cartesian coordinate system fixed at the leading edge. The finest grid resolution in the streamwise direction was 225 grid points from the leading edge to the trailing edge while the finest off-body spacing was 169 points. Removing alternating grid points in one or both directions generated coarse grids. This left 85 points in the off-body direction for the medium grid and 43 points for the coarse grid.

As the grids were coarsened, the wall spacing increased for each grid. This generally causes the laminar wall properties to become less accurate. By decreasing the wall spacing for a given number of grid points in the off-body direction, the stretching ratio between the surface and the outer boundary increases. As the stretching ratio increases, the truncation error of the grid will increase as well. Chan et al[3] showed a stretching ratio below 1.3 is desirable in the off-body direction. Table 2 shows the maximum stretching ratios obtained for the coarse, medium, and fine grids. Based on these values, only the fine and medium grids would be candidates to complete this study since the coarse grid possesses a maximum stretching ratio of 1.56 and 1.4 for the two grid types. The methodology used in the creation of the grids was to set the first 3 cell spacings in the off-body direction to the same value and equispace the last 25% of the points in order to capture any shocks correctly. Between the surface and outer boundary regions the grid points were spaced by a trigonometric stretching function. This stretching function seems to give slightly large stretching ratios, thus future work will be done to try other stretching functions to reduce the maximum stretching ratio.

Parabolic Mesh

The methodology for generating the parabolic mesh was obtained from Roy.[13] This mesh alleviates the singularity at the leading edge and places grid upstream of the leading edge of the plate. The grid can be created from the following mapping:

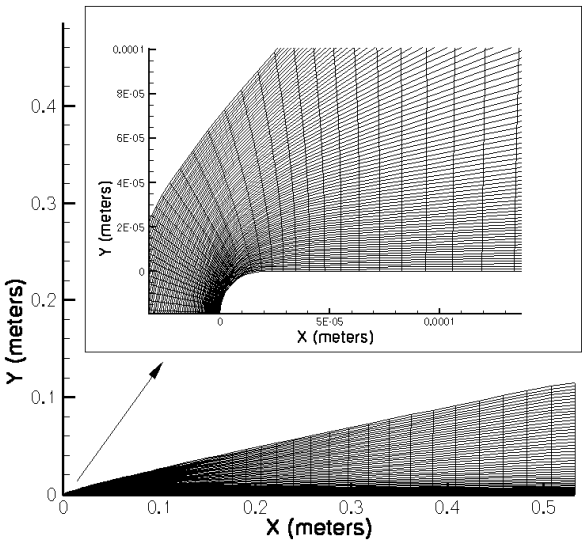

Figure 1. MEDIUM LEADING EDGE GRID

$$x = \alpha(\xi^2 - \eta^2) \quad y = 2\alpha\xi\eta \qquad \alpha = .05$$

$$0 \le \xi \le \xi_{max} \quad 0 \le \eta \le 1 \quad \xi_{max} = \sqrt{1 + 1/\alpha}$$

To implement wall clustering, a transformation on η first proposed by Roberts[14] was used (see also[15]). This transformation assumes that η_{eq} is equispaced from 0 to 1. Here, β is Robert's stretching fuction.

$$\eta = \frac{(\beta+1) - (\beta-1)\left(\frac{\beta+1}{\beta-1}\right)^{1-\eta_{eq}}}{1 + \left(\frac{\beta+1}{\beta-1}\right)^{1-\eta_{eq}}} \tag{2}$$

Based on Roy,[13] a beta value of 1.0001 was used to create the baseline grid. The chosen beta value gave a Re_{cell} of approximately 5.

The boundary conditions for this grid were extrapolation at the exit, freestream at the outer boundary, and symmetry on the $\xi = 1$ gridline.

Finite Radius Leading Edge Mesh

Since the test report listed the leading edge thickness (3.81×10^{-5} meters), a second grid was generated to model the finite radius leading edge with a C-grid topology. The grid was generated so the finest mesh had 225 points over the flat plate section and a minimum of 9 points for the coarsest mesh (36 for the fine mesh) forming the leading edge. Initially, the Re_{cell} of the finest grid was approximately 5. A shock formed at the leading edge of the grid, thus the outer boundary of the grid was adjusted to fit the shock. The C-grid toplogy gives the domain 2 exit planes, which were specified as extrapolation. An image of the baseline grid is pictured in Figure 1.

B. Sphere

Two sphere grids were created, one to be run with the axi-symmetric option and the other to be modeled one quadrant of the sphere (one fourth of the frontal area) with an H-topology taking advantage of symmetry in both y and z. For the axi-symmetric grids, the grid distribution in the streamwise direction was equispaced 33 points. The grid was exteneded in the streamwise direction to 90 degrees from the stagnation point. The axisymmetric grid utilized 65, 85, and 129 off-body points. A Re_{cell} study was done by varying the Re_{cell} from 2 to 10 for the 129 off-body point case to obtain the most accurate wall-spacing. The surface for the 3D grid was generated with identical connectors (65 points) on each axis. These two connectors made up adjacent sides of the H-patch. Eighty-five points were used on the off-body direction. Both grids extended to the same streamwise location.

C. Compression Ramp

Compression ramp grids, which were generated for the 2-D option in OVERFLOW, were generated just like the flat plate grid labeled "finite radius leading edge". A leading edge radius was not defined in the test report, thus the leading edge radius of the flat plate was used to define the leading edge of the compression ramp. This was deemed sufficient because the two models were approximately the same size and the test report labeled the leading edge as sharp. Two cases were ran with a leading edge radius of 1.5 and 2.5 times larger than the flat plate value to verify this assumption. There was virtually no change in the heat transfer or skin friction for the larger radius cases. Standard grid dimensions for this case were chosen as 257 points in the streamwise direction and 85 points of the off-body direction. Several multiples of the streamwise dimensions were explored as well as one one multiple in the off-body direction. The outer boundary was adapted to the shape of the weak shock created by the finite radius leading edge and the downstream compression ramp. Wall spacing was defined by using a Re_{cell} between 1 and 2.

D. X38

X38 grids were built based on the recommendations by Chan et al[3] for overset grid generation. The port side of the vehicle was used with the pitch plane defining symmetry planes on the windward and leeward surfaces. A singular axis (singularity at the nose, C-grid topology wrapped circumferentially around the vehicle) grid was generated to cover the nose to approximately an X/L of 0.5. This allowed for one grid to capture the stagnation region, minimizing overlap of the grids in this high gradient region. It was discovered with initial calculations on the singular axis grid that the grid lines coming out of the pitch plane needed to be perpendicular to the plane in order to provide accurate heat transfer (note that pressures were not affected). Downstream of X/L = 0.5, the overset grid generation technique was utilized to easily grid the body flaps, body flap hingline, rudders, and other detailed geometric features. Seventeen grids were used to model the shape of the X38. An image of the surface grids are given in figure 2. The Re_{cell} for this case was chosen to be 2.

IV. Results

A. Flat Plate

The results for the laminar flowfields were evaluated by computing an RMS error based on the Stanton Number. Computational results were interpolated to the gauge locations so there could be an exact comparison. Two RMS errors were created, one by using the experimental results and the other by using Van Driest's laminar prediction.[7,16,17] For the wind tunnel data, the heating values at each gauge location were averaged over the three runs to get an average wind tunnel value. Equation 3 gives the equation for the RMS error. Note that the exact value can either be the experimental data or Van Driest's laminar prediction.

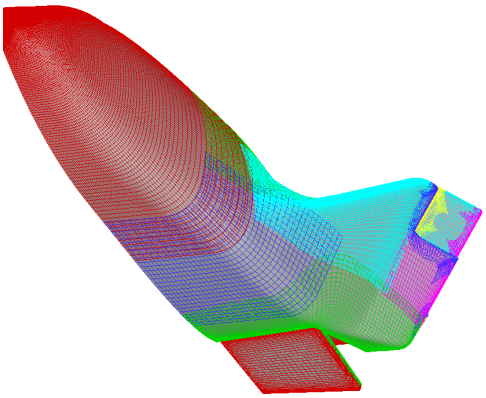

Figure 2. X38 CHIMERA (OVERSET) SURFACE GRID TOPOLOGY

Table 3. RMS ERROR BASED ON GRID AND GRID LEVEL, $Re_{cell} NOTCONSTANT$

	parabolic grid		finite radius	
grid level	WT data	Van Driest	WT data	Van Driest
fine	2.42e-5	2.97e-5	1.09e-5	2.22e-5
combination	2.80e-5	3.42e-5	4.54e-5	6.78e-5
medium	2.83e-5	3.49e-5	4.47e-5	6.56e-5
coarse	3.61e-5	4.38e-5	1.01e-4	1.39e-4

$$RMS = \left(\frac{1}{N} \sum_{i=1}^{N} (St_{i,computed} - St_{i,exact})^2 \right)^{\frac{1}{2}} \tag{3}$$

For the wind tunnel case chosen, the laminar region of the flat plate was approximately 4.0 inches in length. This allowed for comparison to three gauges before the flow became transitional. The third gauge could be considered on the edge of the transition zone, because only one of the three runs at the condition compares well with Van Driest. Because of the lack of laminar wind tunnel data, Van Driest's laminar prediction was the better indicator of an accurate computation.

To begin the study, the medium and coarse grids were generated by removing every other point from the previous grid level. The results of the grid resolution study are listed in Table 3. RMS error is presented as a function of grid type and resolution for the laminar region only. The study shows that the parabolic grid has a more grid converged answer, but the finite radius grid gives a slightly better answer. While doing the resolution study, it was found that it would be optimal to use a fine distribution in the streamwise direction and a medium distribution in the off-body direction. This grid is labeled 'combination' in Table 3.

The results from Table 3 are misleading because, as mentioned earlier the wall spacing for the coarse meshes was obviously larger than the fine mesh. The Re_{cell} of the coarse grids was approximately 15 while the combination and medium grids had a Re_{cell} value of approximately 10. The grid resolution study presented in Table 3 is recreated in Table 4 with a constant Re_{cell} of 5 for each grid. This methodology gave more accurate results based on the RMS value. For consistency, the fine parabolic grid that was created

Table 4. RMS ERROR BASED ON GRID AND GRID LEVEL FOR $Re_{cell} = 5$

	parabolic grid		finite radius	
grid level	WT data	Van Driest	WT data	Van Driest
fine	7.23e-6	1.04e-5	1.09e-5	2.22e-5
combination	9.33e-6	1.18e-5	1.89e-5	3.04e-5
medium	1.14e-5	1.58e-5	1.49e-5	2.30e-5
coarse	5.52e-5	2.32e-5	2.45e-5	3.63e-5

Table 5. RMS ERROR BASED ON Re_{cell} FOR THE COMBINATION GRID

	parabolic grid		finite radius	
grid level	WT data	Van Driest	WT data	Van Driest
Re_{cell}=1	9.5e-6	1.13e-5	5.51e-6	3.43e-6
Re_{cell}=2	6.87e-6	5.57e-6	6.11e-6	6.00e-6
Re_{cell}=5	9.33e-6	1.18e-5	1.89e-5	3.04e-5
Re_{cell}=10	6.07e-5	7.99e-5	6.06e-5	8.78e-5

with a β value of 1.0001 was run through the same grid adjustments as the other grids. Surprisingly, this modification lowered the RMS error for the fine parabolic grid significantly. The decrease in the RMS error can be attributed to the modified grid having a different stretching function coming off the wall, therefore having more points in the boundary layer (larger spacing near the outer boundary). Based on Table 4, the combination grid was chosen to complete the study. Table 5 shows the combination grid for varying Re_{cell} from 1 to 10. The results show that by decreasing the Re_{cell} to 2 the error in the heating prediction is at a minimum. Figure 3 shows the combination grids for both grid types compared to the data and theory for a Re_{cell} of 2 and 5.

B. Sphere

Stagnation heating results were the only obtainable measurement in the wind tunnel. Therefore comparisions to the data were done by looking at percent error in the stagnation heating calculation. A positive percent error indicates an underprediction of the stagnation heat transfer. Table 6 presents the percent error of each case (note an 'N/A' represents a calculation that was not attempted). Results for the sphere case are consistent with the other test cases in that the larger Re_{cell} values underpredict the correct heat transfer while the lower values around two provide a good comparison to the experimental results. Sixty-five off-body points with a Re_{cell} gives a nearly acceptable prediction, but the 85 off-body point case has the most accuarte heating prediction. Also, the axi-symmetric case shows that 85 off-body points are sufficient to predict stagnation heating. Overall, the computations compare very well to the wind tunnel data, with the minimum percent error being -0.18%. None of the sphere results experience any problems with the 'carbuncle' problem seen in some blunt body flowfields.

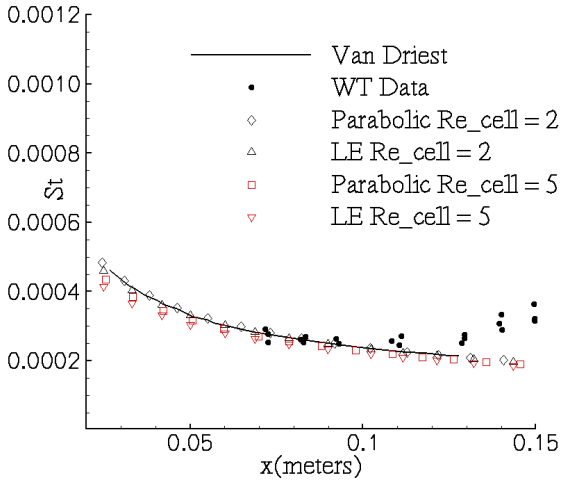

Figure 3. FLAT PLATE LAMINAR HEATING COMPARISION Re_{cell}=2,5

Table 6. PERCENT ERROR IN AXI-SYMMETRIC AND 3D SPHERE CALCULATIONS

grid	*Recell*		
dimension	10	5	2
axi - 33x65	33.1	15.2	-1.5
axi - 33x85	33.1	13.6	-0.18
axi - 33x129	33.1	15.5	-0.4
3D - 65x65x85	N/A	N/A	-0.85

C. Compression Ramp

One of the most important characteristic of the compression ramp is the prediction of the laminar separated region. Therefore, qualitative comparisons of stanton number and skin friction coefficient were used to assess the results. To quantify the comparisons for the compression ramp the RMS error was not used. Quantitative measurements of the separated region were attempted, but the wind tunnel data lacked the resolution for an accurate comparison. Skin friction was much more sensitive to grid resolution than Stanton Number. Therefore skin friction was used to define a grid converged result. Figure 4 shows the skin friction coefficient for two grid resolution studies. Streamwise resolution was first explored with 129, 257, and 513 points for 85 off-body points. The results for Cf are grid converged for 257 and 513 streamwise grid points. Off-body resolution was explored last, with 65, 85, and 129 points used with 257 streamwise grid points. The results show that the solution did not reach grid convergence, although the 85 off-body points compared very well with the wind tunnel data. This discrepancy is currently being explored. A heating distribution is presented in figure 5 for the 257 x 85 grid case. Stanton number agrees very well in the separated region but is slightly off on the compression ramp section.

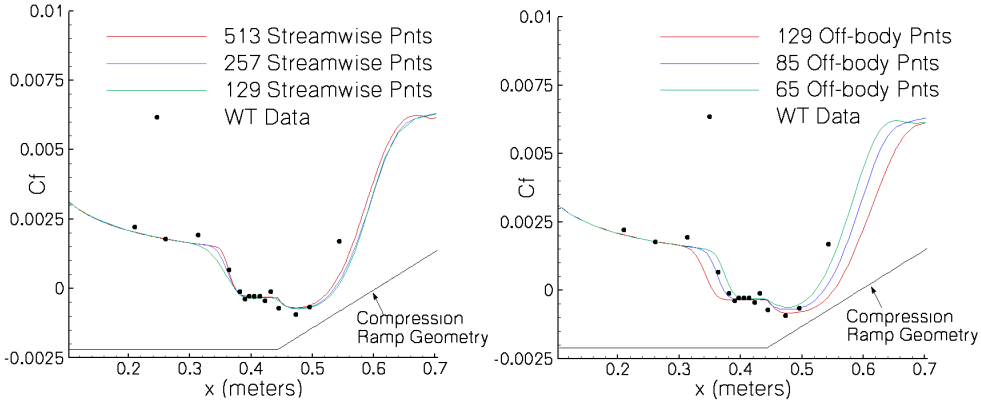

Figure 4. STREAMWISE AND OFF-BODY GRID RESOLUTION STUDY - SKIN FRICTION

D. X38

Nearly all the X38 Wind Tunnel data in existence is export controlled. Therefore it is not in the public domain. Horvath et al[11] published centerline heating cuts at Mach 6. Those are the only comparisons made here. Figure 6 shows the non-dimensionalized heat transfer for this Mach 6 condition from the nose to an X/L location of approximately 0.6. The heat transfer data has been nondimensionalized by a stagnation heating value. The results show excellent agreement. More detailed geometric comparisons have been made at other conditions and on other regions of the vehicle including the body flaps and body flap cavity that show similiar agreement, but these are export controlled. Although not pictured, the heating across grid boundaries was smooth and continuous. Olsen et al[4] had problems with heat transfer continuity across grid boundaries on the X33. The current X38 grids were created with more than minimal overlap (atleast 5 points of overlap for each grid) while the X33 grids were created with minimal overlap. Figure 7 shows heat transfer contours for a hypersonic flow. The black lines on the image are overset grid boundaries. Note the smooth contours across overlapping grid boundaries. This extra overlap could be the difference in the smooth heat transfer across overlapping grid boundaries. For this case more than any other, slowly changing the four dissipation parameters was essential in providing a converged result. Without ramping, the coefficients the solution would not converge.

V. Conclusion

This work extends OVERFLOW's current capabilities to the prediction of hypersonic perfect gas flowfields. By using the matrix dissipation models, solutions have been shown to yield comparable results to an upwind biased TVD scheme with less computational cost. The values of DIS2, DIS4, VEPSN, and VEPSL proposed by Olsen have been shown to provide viable results. By ramping these coefficeints from their initial startup values to their correct ones, solutions over complex three-dimensional bodies converge very smoothly. The X38 results showed the feasibility of using the overset grid topology to obtain surface heat transfer. By using at least 5 points of overlap and by following general overset grid practices[3] continuous surface heat transfer was obtained. Further work will be done in this area for data that is not ITAR restricted so heat transfer on overset grids can be published.

Values of Re_{cell} between 1 and 2.5 were shown to provide accurate heat transfer results for off-body spacings of 85. These values should serve as a guideline for future computations when laminar boundary layer properties are required. The Re_{cell} values needed for OVERFLOW are slightly lower than what

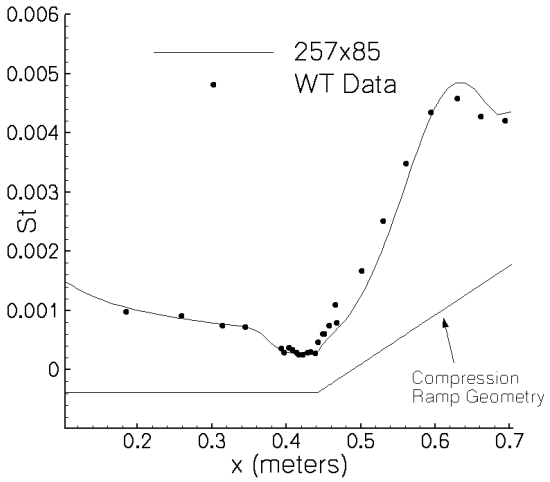

Figure 5. STANTON NUMBER FOR 257 X 85 GRID POINT CASE

Gnoffo[12] reported, although one could expect differences between how wall properties are evaluated between finite volume and finite difference codes. Overall the slightly lower Re_{cell} values seem reasonable. Off-body grid distributions were examined with 85 points being the converged up value. Nearly every test case gave the lowest error for 85 points. This number of points along with the Re_{cell} values found generally give stretching ratios below 1.2 in the off-body direction.

References

[1]Jespersen, D. C., Pulliam, T. H., and Buning, P. G., "Recent Enhancements to OVERFLOW," *AIAA 35th Aerospace Sciences Meeting, Reno, NV*, January 1997, AIAA 97-0644.

[2]Buning, P., Jespersen, D., Pulliam, T., Klopfer, G., Chan, W., Slotnick, J., Krist, S., , and Renze, K., *OVERFLOW User's Manual, Version 1.8s,*, NASA Langley Research Center, 2000.

[3]Chan, W. M., Gomez, R. J., Rogers, S. E., and Buning, P. G., "Best Practices in Overset Grid Generation," *32nd AIAA Fluid Dynamics Conference, St. Louis, MO*, June 2002, AIAA 2002-3191.

[4]Olsen, M. E. and Prabhu, D. K., "Application of OVERFLOW to Hypersonic Perfect Gas Flowfields," *15th AIAA Fluid Dynamics Conference, Anaheim, CA*, June 2001, AIAA 2001-2664.

[5]Swanson, R. and Turkel, E., "On Central-Difference and Upwind Schemes," Tech. Rep. 182061, NASA Langley Research Center, Hampton, VA, June 1993, NASA Contractor Report (ICASE).

[6]Miller, C. G., "Langley Hypersonic Aerodynamic/Aerothermodynamic Testing Capabilities - Present and Future," June 1990, AIAA 90-1376.

[7]Cary, A. M., *Turbulent Boundary Layer Heat Transfer and Transition Measurements With Extreme Surface Cooling in Hypersonic Flows*, MS Thesis, University of Virginia, Charlottesville, VA, August 1969.

[8]Chadwick, K. M., "Stagnation Heat Transfer Measurement Techniques in Hypersonic Shock Tunnel Flows over Spherical Segments," *32nd AIAA Thermophysics Conference, Atlanta, GA*, June 1997, AIAA 97-2493.

[9]Holden, M. S., "A Study of FLow Separation in Regions of Shock Wave-Boundary Layer Interaction in Hypersonic Flow," 1978, AIAA 78-1169.

[10]Grasso, F., Marini, M., and Passalacqua, M., "Numerical Solution of Hypersonic Flows with Zonal Mesh Enrichment," *Hypersonic Flows for Reentry Problems*, edited by R. Abgrall, J.-A. Desideri, R. Glowinski, M. Mallet, and J. Periaux, Vol. 3, INRIA-GAMNI/SMAI, Springer-Verlag, New York, April 1991, pp. 392–406.

[11]Horvath, T. J., Berry, S. A., Merski, N. R., and Fitzgerald, S. M., "X-38 Experimental Aerothermodynamics," *34th AIAA Thermophysics Conference, Denver, CO*, June 2000, AIAA 2000-2685.

[12]Gnoffo, P. A., Gupta, R. N., and Shinn, J. L., "Conservation Equations and Physical Models for Hypersonic Flows in Thermal and Chemical Nonequilibrium," Tech. Rep. 2867, NASA Langley Research Center, Hampton, VA, February 1989.

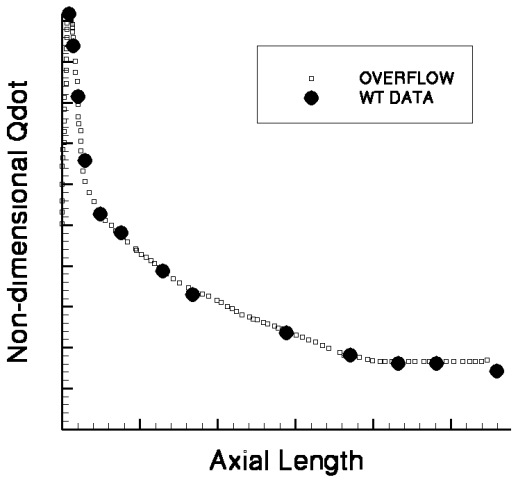

Figure 6. NON-DIMENSIONALIZED X38 HEAT TRANSFER

[13]Roy, C. J. and Blottner, F. G., "Assessment of One- and Two-Equation Turbulence Models for Hypersonic and Transitional Flows," *AIAA 38th Aerospace Sciences Meeting, Reno, NV*, January 2000, AIAA 2000-0132.

[14]Roberts, G. O., "Computational Meshes for Boundary Layer Problems," *Lecture Notes in Physics*, Vol. 8, Organization, Springer-Verlag, New York, 1991, pp. 171–177.

[15]Tannehill, J. C., Anderson, D. A., and Pletcher, R. H., *Computational Fluid Dynamics and Heat Transfer*, Taylor & Francis, Bristol, PA, 1997.

[16]Driest, E. V., "Investigation of Laminar Boundary Layer in Compressible Fluids Using the Crocco Method," January 1952, NACA TN 2597, 1952.

[17]Monaghan, R., "An Approximate Solution of the Compressible Laminar Boundary Layer on a Flat Plate," November 1949, RAE Tech. Note Aero. 2025, 1949.

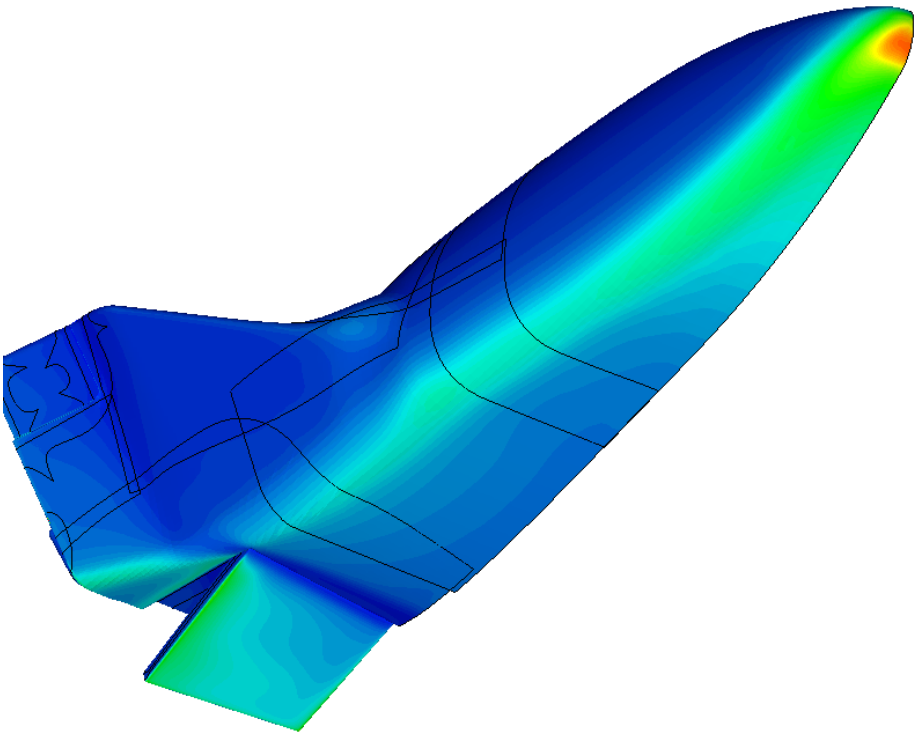

Figure 7. HEAT TRANSFER CONTOURS OVER THE X38